Synthesis, molecular structure, vibrational studies, optical properties and electrical conduction mechanism of the new hybrid compound based on selenate

Ikram Dhouib, Ali Ouasri, Philippe Guionneau, Stanislav Pechev, Zakaria Elaoud

Synthesis, molecular structure, vibrational studies, optical properties and electrical conduction mechanism of the new hybrid compound based on selenate

Ikram DHOUIB[a*], Ali OUASRI[b], Philippe GUIONNEAU[c], Stanislav PECHEV[c], Zakaria ELAOUD[a]

[a]*Laboratory of Physical-Chemistry of Solid State, University of Sfax, Faculty of Sciences of Sfax, Tunisia.*

[b]*Laboratoire (LReSIV); Centre Régional des Métiers de l'Education et de la Formation, Madinat Al Irfane, Souissi, BP 6210 Rabat, Morocco.*

[c]*CNRS, Univ. Bordeaux, ICMCB, 87 avenue of Dr A. Schweitzer, 33608 Pessac, Bordeaux, France*

AUTHOR INFORMATION

*Corresponding author: DHOUIB Ikram

- Tel: +21697019206, Sfax Faculty of Sciences, Chemistry Department, Soukra Road km 3,5 - B.P. 1171, 3018 Sfax – Tunisia.
- E-mail address: ikramdhouib82@yahoo.fr

Abstract

The new hybrid material tetrapropylammonium hydrogen selenate bis (selenic acid), $N(C_3H_7)_4[HSeO_4][H_2SeO_4]_2$ (hereafter abbreviated TPSe) has been synthesized by slow evaporation technique at room temperature. Crystal structure, DTA-TGA measurements, Raman, Infrared spectroscopy, nuclear magnetic resonance (NMR) electrical properties, and optical properties were provided to characterize the TPSe. This crystal structure contains one organic cation $[N(C_3H_7)_4]^+$, one $[HSeO_4]^-$ tetrahedra, and two neutral selenic acids H_2SeO_4. The inorganic $[HSeO_4]^-$ and H_2SeO_4 species consist of infinite two-dimensional inter-linkers via strong hydrogen bonds (O-H…O), giving birth to trimmers $[(H_2SeO_4)_2\ HSeO_4]_n^{n-}$. The IR and Raman spectra of the compound recorded at room temperature were studied in regard to the literature data, and on the basis of theoretical group analysis. The theoretical calculations using the density functional theory DFT at the B3LYP/6-31G(d) level, are made to study the optimized molecular structure, the vibrational spectra, and the optical properties of TPSe compound. Good agreements were found between the theoretical results and the experimental Raman, IR spectra and the molecular structure. The polarizability α, the hyperpolarizability β, and the electric dipole μ calculated using DFT/B3LYP-31G(d) exhibit the non-zero hyperpolarizability β of the TPSe, indicating that this material could be used in certain NLO applications. The thermal DTA-TGA analyses did not show any phase transition in the 333-500 K temperature domain. The complex impedance spectroscopy is measured and discussed in the temperature (290-363K) and frequency (1kHz -13MHz) domains to study the electrical propreties of the compound.

Keywords: Tetrapropylammonium, structural analysis, DFT calculations, NLO, impedance spectroscopy, conduction mechanism.

1. Introduction

During the two past decades, great importance has been paid to the organic–inorganic hybrid materials (IO), which have been found to present important properties such as electronic, nonlinear optical, magnetic, luminescence and ferroelectric [1-8]. While the needs of NLO materials has been increased, and has attracted the attention of many researchers because of their great applications in different fields like in optical communication, optoelectronics, laser technology, optical data storage, photonics, and optical signal processing [9-14]. These physical properties depend on the used inorganic acids with organic compounds; therefore considerable efforts have been made to produce materials having a non-centrosymmetric cell, strong non-linear optical coefficients, and large polarizability. In recent literature of theoretical and experimental studies are appropriate to the organic, inorganic, and organic-inorganic NLO materials. Due to the structure flexibility, the ability to form multidirectional hydrogen interactions and the reports of macroscopic and microscopic responses non-linearity property, tetra-alkylammonium cations of the general formula $(C_nH_{2n+1})_4N^+$, such as $(CH_3)_4N^+$, $(C_2H_5)N^+$, $(C_3H_7)N^+$, are one of important organic parts which were selected to synthesis nonlinear materials. Recently, the specific geometry of these cations can generate supramolecular networks in one (1D), two (2D) or three (3D) dimensions. Besides, numerous stabilized compounds belonging to the $[(R)_4N](HXO_4)$, $[(R)_4N](HXO_4)(H_2XO_4)_2$, $[(R)_4N]\ (H_2XO_4)(H_3XO_4)_2$ families (where R= CH_3, C_2H_5, C_3H_7, and X = Se, S, As, P) present interesting physical properties such as electrical conductivity, vibrational spectroscopy, theoretical calculations, and non-linear optical properties [15-20].

The present work focuses on the synthesis and the study of a new organic-inorganic $N(C_3H_7)(HSeO_4)(H_2SeO_4)_2$ compound. Then, the results of the structural study by X-ray diffraction, vibrational spectroscopy, NLO response as well as DFT calculations, NMR characterization, thermal analysis, and electrical properties, are discussed in this paper.

2. Experimental

2. 1. Synthesis

All chemicals and solvents were traded from Sigma-Aldrich; single crystals are synthesized at room temperature (29°C) by slow evaporation method.

The reaction mixture obtained was prepared from an aqueous solution of selenic acid H_2SeO_4 (144.97 g /mol, 1.407 g/cm3, purity 99.95% SIGMA ALDRICH) and tetrapropylammonium hydroxide $(C_3H_7)_4NOH$ (203.37g /mol, 1.012 g/cm3, purity 100% SIGMA ALDRICH) and mixed magnetically for 1 hour. After the agitation, the solution was left to slowly evaporate at room temperature. Following a period of about fifteen days, colorless transparent parallelepiped TPSe crystals were isolated from the solution. This synthesis method was enough effective to have high-quality crystals of the material with a good yield. As the crystals are hygroscopic, therefore the method of crystal growing was carried out in the desiccator with the P_2O_5. The synthesis reaction scheme of TPSe is given in the following equation:

$$(C_3H_7)_4NOH + 3H_2SeO_4 \longrightarrow N(C_3H_7)_4[HSeO_4][H_2SeO_4]_2 + H_2O$$

The density of the synthesized compound was measured at room temperature by pycnometry by flotation in toluene. The mean value of the measured density, $D_m = 1.623$, is in good accordance with that obtained from the crystal-structure determination (see in Table 1).

2. 2. X-ray data collection

A suitable single crystal of the title compound with sizes of 0.28×0.17×0.10 mm^3 has been carefully selected under an optical examination for structure determination. The data file managed was using a Bruker Kappa CCD diffractometer with graphite-monochromated Mo Kα radiation (λ = 0.71073Å) was used in order to study its structural analysis. The crystal structure has been resolved by direct methods using SHELXS-97 [21], and has been refined by full-matrix least square with SHELXL-97 [22]. The detailed crystallographic data and structure refinement parameters are listed in Table 1. All the hydrogen positions were fixed

geometrically, with (O-H = 0.82 Å and C–H = 0.96–0.97Å), the structure analysis has been carried in the monoclinic symmetry, according to the auto-methods search for space group available in the WINGX environment [23]. All figures were made using DIAMOND program [24]. Crystallographic parameters for the structural analysis reported in this work are also deposited in Cambridge Crystallographic Data Centre and can be freely accessed at www.ccdc.cam.ac.uk (CCDC no. 1584929).

2. 3. Spectroscopic measurements

At room temperature, the vibrational measurements were carried out. The infrared absorption (FT-IR) spectrum of TPSe was recorded in the range 4000-400 cm^{-1}, on a PERKIN-ELMER FT-IR spectrometer. Samples were diluted with spectroscopic grade KBr and pressed into a pellet, with a spectral resolution of 2 cm^{-1}. The Raman spectrum (FT-Raman) of this compound was recorded using Horiba Jobin Yvon LabRAM HR 800 Dual Spectrophotometer. The excitation line was the 630 nm from a Neon laser in the range 50-4000 cm^{-1}. The laser beam was focused on the sample through a 50× LF objective microscope and the incident power was limited to 5 mW to avoid sample heating degradation.

The NMR–magic-angle spinning (MAS) experiments have been done at room temperature on a Bruker WB 300 MHz. Then, the powdered sample was wrapped in a 4 mm diameter rotor and set to rotate at a speed up to 8 kHz in a Doty MAS probe head. The ^{13}C spectrum was collected by a cross-polarization of the proton with 15.6 μs contact time.

The crystals TPSe are grinded and were pressed at room temperature under 200MPa stress, giving into a cylindrical pellet of 10mm in diameter and 1.9mm in thickness. The Measurements of the electrical transport properties of this compound were measured on this pellet in the frequency range of 1 kHz to 13 MHz frequency using a Hewlett-Packard 4192 ALF automatic bridge monitored by an HP Vectra microcomputer. The measurements were done over the temperature range of 290–373K.

2. 4. Computational details

The geometry and frequencies of TPSe were obtained from the density functional (DFT/B3LYP) with the 31G(d) level basis set. Any, the calculations have gone to an optimized geometry which, coincides to a true energy minimum disclosed by the absence of imaginary values in the wavenumbers calculations. All these calculations were employed using the Gaussian 03 program [25]. Vibration modes assignments have been expressed by visual inspection of eigenvectors animated using the Molekel program [26] and as well by comparison with the results of the similar compounds.

2. 5. Thermal analysis

Setaram thermoanalyser, TGA-DTA92 (Pt crucibles, Al_2O_3 as a reference) under air flow (100ml/min), was used to make thermal analyses of the sample TPSe. The TGA-DTA thermograms were made with 21.35 mg in a closed capsule from 333 K to 500 K for this hygroscopic sample; with heating rate of 5 °C mn^{-1}.

3. Results and discussion

3. 1. Structural analysis

The novel compound TPSe belongs to the monoclinic space group Ia (Z=4) with the lattice parameters: a = 7.3160(2) Å, b = 31.7630(4) Å, c = 8.6890(2) Å, β = 95.340(2)°. The representation of the basic unit of the material (Figure 1a) is formed up of one protonated cation $[(CH_3CH_2CH_2)_4N]^+$, one $[HSeO_4]^-$ anion and two neutral selenic acids H_2SeO_4, all placed in general positions, corresponding to the Wyckoff position (4a) of the Ia space group. Figure 2 illustrates that the organic groups alternate with those of the inorganic groups along the c axis. The geometry of the cation presents a broken cross configuration, and shows that is formed by four aliphatic carbon chains parallel to the c direction and is located at at z = ¼ and z = ¾. Whereas the inorganic layer is built up by infinite chains of $[(H_2SeO_4)_2HSeO_4]^-_n$ anions parallel to the [010] direction. The midplanes of these selenates groups, are located at z = ¼

and z = ¾. Whereas the inorganic layer is built up by infinite sheets of trimmers $[(H_2SeO_4)_2HSeO_4]^-$ as seen in Fig.3. These groups bonded together by strong interlayer O-H…O hydrogen bonds and contribute to the cohesion of the structure. In the tetraethylammonium selenate $N(C_2H_5)_4[HSeO_4][H_2SeO_4]_2$ (TESe) crystallized in the Cc (Z=4) space group [a=19.705(1) Å; b=7.5420(3) Å; c=19.199(1) Å, β =115°] [20], the $[HSeO_4]^-$ and H_2SeO_4 forming $[(H_2SeO_4)_2HSeO_4]^-_n$ layers tetrahedra planes, and alternating with the $^+N(C_2H_5)_4$ organic groups planes, have been found to be perpendicular to the *a*-axis.

In the tetraalkylammonium selenates, the negative charge of the anionic species is generally contra balanced by the positive charge of the organic cation. In the TPSe compound, the Se atom is four-fold coordinated by terminal oxygen atoms and forms two tetrahedral $[HSeO_4]^-$ and $[H_2SeO_4]$, forming a tetrahedral arrangement. Indeed, within the first selenate tetrahedron, the Se-O distances range from 1.559(1) Å to 1.617(2)Å. Such coordination geometry is typical of selenate groups and was observed in the structures of $N(CH_3)_4HSeO_4$, $C_{12}H_{12}NHSeO_4$, $C(NH_2)_3HSeO_4$, and $N(C_2H_5)_4[HSeO_4][H_2SeO_4]_2$ [20, 27- 29].

For the second tetrahedron, the Se-O distances range from 1.524(12) Å to 1.656(11) Å; in the $K(HSeO_4)(H_2SeO_4)$ and $Cs(HSeO_4)(H_2SeO_4)$ compounds [30], the H_2SeO_4 groups have a similar coordination geometry. Moreover, the O-Se-O bond angles vary from 104.2(7) to 114.7(5) of $[HSeO_4]^-$ and from 102.4(8) to 116.2(7) of H_2SeO_4, which suggests a slight distortion of $[HSe(1)O_4]^-$; $H_2Se(2)O_4$ and $H_2Se(3)O_4$ tetrahedra. The deformation of the square planar is probably resulting from hydrogen bond interactions. In the crystal structure, the tetrahedra of $[HSeO_4]^-$ and $[H_2SeO_4]$ show an extensive network made of strong hydrogen bonding O–H•••O, due to numerous acceptor and donor atoms, which give rise to trimmers, made up of $[(H_2SeO_4)_2HSeO_4]^-$ as seen in Figure 3. In the present TPSe compound, the various hydrogen bond parameters vary from 2.29(2) Å to 2.42(2) Å for d(D…A), as summarized in Table 2. While in the TESe compound studied recently [20], the same

parametrs are ranging from 2.480(16) to 2.480(16), which implies clearly that the hydrogen bonding are more strong in the TPSe rather than in the TESe.

Within the organic cation, the C-C bond lengths values vary from 1.38(3) to 1.47(2) Å, the C-N distances vary from 1.43(2) to 1.45(2)Å, and the C-C-C, N-C-C angles are between 102.5 (13)° and 121.4 (16)°. The obtained values do not show remarkable defects, since they are in good agreement with the data of compounds having a linear chain [15-20].

To interpretate theoretically the structural and vibrational properties of the material, we have used the density functional theory (DFT), which is a cost-effective general procedure for interpreting. The optimized geometry of the title material model is displayed in Figure 1b. The measured bond lengths and bond angles together with the calculated ones are enunciated in Tables 3 and 4. After an attentive comparison, a good coherency between the bond lengths calculated and experimental of the molecular structure is found.

3. 2. Vibrational studies of $N(C_3H_7)_4[HSeO_4][H_2SeO_4]_2$

The Infrared and Raman spectra of $N(C_3H_7)_4[HSeO_4][H_2SeO_4]_2$ have been recorded at room temperature (Figures 4 and 5). The assignement of the observed bands, arising from the internal vibrations of organic cations, selenate species, and O−H•••O hydrogen bonds, is supported by developing the density functional theory DFT (B3LYP/6-31G(d)) frequencies calculations of the TPSe compound. The obtained theoretical IR and Raman spectra are associated and compared to experimental spectra (Figure 4, and 5). The different vibrational modes have been realized by the visual inspection of animated modes by using the Molekel program [26], and then compared with precedent experimental and theoretical results mentioned in the literature for similar compounds [31-32]. Reliable correspondences between experimental and calculated frequencies were made. The Table 5 contains the wavenumbers and the purposed bands assignments. Furthermore, the theoretical group analysis is used to

predict the different species vibrational modes, which could be Raman and Infrared actives in the TPSe crystal.

* $[HSeO_4]^-$ and H_2SeO_4 vibrational modes

The free $[SeO_4]^{2-}$ anion considered in T_d symmetry posses 9 internal vibrational modes described as: A_1 (Ra) + E (Ra) + $2F_2$ (Ra, IR), which correspond to two stretching modes $\nu_1(A_1: \nu_s$ Se-O), $\nu_3(F_2: \nu_{as}$ Se-O), and two bending modes ν_2(E: δ_s O-Se-O), $\nu_4(F_2: \delta_{as}$ O-Se-O).

The free $[H_2SeO_4]$ and $[HSeO_4]^-$ groups are considered in C_{2V} and C_{3v} symmetry, respectively. Inside the crystal, these species are too situated in the general sites of symmetry (C_1). Of the 15 internal modes ($6A_1$ + 4 B_1 + $2A_2$ + 3 B_2) of $[H_2SeO_4]$ described in its symmetry C_{2v}, nine are due to the vibrational modes (A_1 + E + $2F_2$) of the free $[SeO_4]^{2-}$ considered in T_d symmetry, and 6 vibrations (4 A_1 + 2 B_1) coresponding to OH vibrations of H_2SeO_4 in C_{2v} symmetry. The site symmetry correlation leads to 9 (A) modes due to the $[SeO_4]^{2-}$ anion, and six (A) modes of OH groups of $[H_2SeO_4]$ (Table 6).

In the same way, among the 12 internal modes ($4A_1$ + $2A_2$ + 3E) of the $[HSeO_4]^-$ taken in its C_{3v} symmetry, nine are associated with the vibrational modes ($3A_1$ + 3E) of the $[SeO_4]^{2-}$ of T_d symmetry, and three (A_1 + $2A_2$) with OH vibrations of $[HSeO_4]^-$ in C_{3V} symmetry. The site symmetry approach (Table 7) leads to nine (A) modes of the $[HSeO_4]^-$ and three vibrations (A) associated to the OH group of $[HSeO_4]^-$.

In fact the representation of the $[(H_2SeO_4)_2HSeO_4]^-$ vibrational modes illustrated in the Table 8 predicts 27 (A) vibrational modes coming from SeO_4^{2-} groups ($5A_1$ + 5E + $4F_2$), and 15 (A) modes originated by OH groups of H_2SeO_4 and $[HSeO_4]^-$. All these modes should be active as well as in Raman and Infrared spectra.

It is to note that the free selenate ion SeO_4^{2-} of T_d symmetry leads to four fundamentals normal modes: ν_1 (A_1) = 837 cm^{-1} and ν_2 (E) = 345 cm^{-1} actives in Raman, and ν_3 (F_2) = 873 cm^{-1} and ν_4 (F_2) = 413 cm^{-1}, too Raman and Infrared actives [15]. In the selenate stretching

modes region, the asymmetric stretching mode of the selenate anion ν_3 [ν_{as} (Se-O)], is observed of one strong band in the Raman spectrum at 918 cm^{-1} and a weak band in the IR spectrum at 845 cm^{-1}, and a weak band in the IR spectrum at 845 cm^{-1}, which is assigned to the symmetric stretching mode ν_1 [ν_s (Se-O)] of this anion. It is worthy to note that no bands are observed in the Raman spectrum of the title compound in the frequency range of the symmetric vibrational modes ν_1 (A_1), actives theoretically in Raman as well as in H_2SeO_4 (C_{2v}), $[HSeO_4]^-$ (C_{3v}) and $[SeO_4]^{2-}$ (T_d). The internal vibrational modes of "isolated selenate" are considerably differents from those of the hydrogen selenate species. The most characteristic is the medium band appeared at around 765 cm^{-1} due to the stretching ν(Se–OH) of the longest Se-OH bonds in the $[HSeO_4]^-$ and H_2SeO_4 species, which is considered as a component of the ν_3 [ν_{as} (Se-O)] [33].

In the bending modes region, the band of medium intensity observed in the Raman spectrum at 420 cm^{-1} and the two weak bands observed in the Infrared spectrum at 425 at 470 cm^{-1} can be assigned to the asymmetric bending modes ν_4 [δ_{as} (O-Se-O)]. The observation of two Infrared components in this region may be due to the splitting of the degenerate modes $\nu_4(F_2)$ under the site symmetry effect. This observation is an indication that the selenate species $[HSeO_4]^-$ and H_2SeO_4 are distorted in the compound. The symmetric mode ν_2 [δs (O-Se-O)] is observed with a weak band in the Raman spectrum at 275 cm^{-1}even if it is shifted from the known region (320-340 cm^{-1}) mentioned in the litterature for the ν_2 (E) selenate vibrations [33, 15]. The weak band observed in the Infrared spectrum at 1000 may be due to the "out-of-plane bending" SeOH, i.e. γ(OH) modes coming from the $[H_2SeO_4]$ and $[HSeO_4]^-$ species. While the "in-plane bending" δ(OH) vibrational modes of these species are observed as strong Infrared bands at 1600 and 1645 cm^{-1}, and as a weak Raman band at 1600 cm^{-1}. The δ(OH) modes may be either the origin of the medium Infrared band appeared at 1300 cm^{-1}, and the Raman one observed at 1299 cm^{-1} in Raman.

In the Raman spectrum of the title compound, the strong band appeared as a doublet around 100 cm^{-1} is undoubtedly due to the external vibrational modes (lattice modes), especially to the rotational modes. The strong intensity of this band suggests the important rotational motions in the title compound, and this could affected the neighbouring internal vibrational modes ν_2 [δ_s (O-Se-O)] of $[(H_2SeO_4)_2HSeO_4]^-$ anions, which are not observed in its known region (320-350 cm^{-1}).

* Vibrational modes of $[(CH_3CH_2CH_2)_4N]^+$ cations

The free tetrapropylammonium is considered to be of S_4 symmetry. So, the internal vibrational modes of this cation are determined as: 29 A (Ra) + 30 B (Ra, IR) + 29 E (IR, Ra). In the structure of the title compound [space group Ia (Z=4)], the tetrapropylammonium cations are observed in positions generals corresponding to the sites of symmetry C_1. The change in symmetry from S_4 to C_1 gives for each cation 117 A vibrational modes in the site group (Table 9). Each of these vibrations should split into two components in the group factor C_{2h}, giving 117 A'+ 117 A''modes, all Raman and infrared actives.

The internal vibrational modes of the tetrapropylammonium cations are assigned by comparison with like compounds [34–41]. As predicted by the theoretical group analysis, all the cationic modes are active as well as in Raman and Infrared spectra.

In the C-H spectral region (2800-3100 cm^{-1}), the IR and Raman spectra present weak and broad bands. Indeed, in the IR spectrum, the weak Infrared band appeared at (2995 cm^{-1} is assigned to the asymmetric stretching modes $\nu_{as}(CH_2)$ and $\nu_{as}(CH_3)$; the band observed at 2925 cm^{-1} is due to the symmetric stretching modes $\nu_{as}(CH_2)$ and $\nu_{as}(CH_3)$. In the Raman spectrum, the asymmetric modes of these groups appear as a weak band at 3072 cm^{-1}, 2956 cm^{-1} in the Raman spectrum, while the symmetric modes $\nu_s(CH_2)$ and $\nu_s(CH_3)$ give rise to medium and broad band at 2900 cm^{-1}. At low frequencies (2700-1700 cm^{-1}), the Raman spectrum presents several bands of different intensities (Table 5). Excepted for the strong

band observed at 2435 cm^{-1}, the medium band at 2650 cm^{-1}, and the weak bands at 2290 cm^{-1}, which could be due to the ν (O-H----O) corresponding to the hydrogen bonding effect in the compound [33]; the remaining bands, generally of weak intensities can be originated from the non-fundamental modes.

In the 1630-400 cm^{-1} spectral region, the band of medium intensity observed in the Infrared spectrum at 1488 cm^{-1} is assigned to the asymmetric deformation modes $\delta_{as}(CH_3)$ and $\delta_{as}(CH_2)$, which did not appear in the Raman spectrum. The medium Infrared band observed at 1400 cm^{-1}, and the weak Raman band appeared at 1393 are due to the symmetric deformation modes $\delta_s(CH_3)$ and $\delta_s(CH_2)$. The twisting modes $t(CH_2)$ give rise one weak band at 1297 cm^{-1} in the Raman spectrum and two bands (1324, 1300 cm^{-1}) in the Infrared spectrum, and the rocking ρ_r (CH_3) vibration modes are observed as two medium bands, at 1200 cm^{-1} in the Raman spectrum, and at 1195 cm^{-1} in the infrared spectrum. The skeletal stretching modes [ν(C-N), ν(C-C)] and the bending skeletal ones [δ(N-C-C)/ δ(C-C-C)] are observed in the Infrared and Raman spectra of this compound over the spectral range (1130 - 400 cm^{-1}) as illustrated in the Table 5. To note that below 1000 cm^{-1}, are observed the internal modes of the $[HSeO_4]^-$ and H_2SeO_4 species, which certainly made the bands assignement in this region more difficult.

* Hydrogen bonding vibrations (3100-3850 cm^{-1})

In this region of the IR and Raman spectra of TPSe compound, appeared several bands of weak to medium intensities, as given in the table 5. The assignement of such bands seems to be difficult, since two types of OH vibrational modes are involved in this region: the ν(OH…O) modes due to the hydrogen bonding in the crystal, and the stretching modes ν(OH) of the selenate $[HSeO_4]^-$ and H_2SeO_4 species, which are not implied in the hydrogen bonding. Hence, the medium bands located at 3540 cm^{-1} in the infrared spectrum, and at (3825, 3530 cm^{-1}) in the Raman spectrum may be due to the stretching modes ν(OH), which are rarely

observed in the litterature above 3700 cm^{-1}. The criterion for a free OH is a narrow band with a significant intensity and a weak dependence on the medium. The harmonic modes may be seen in this region, but especially if strong vibrational bands are observed at around 1400 cm^{-1}, which is not stated in the TPSe compound, characterized by weak bands near 1400 cm^{-1}; this favourites the assumption assigning the observed band at 3800 cm^{-1} to the stretching O-H of selenate species. To note that the explanation provided here needs to be investigated carefully by studying the deuteration effect on the OH stretching modes.

The calculated DFT frequency of the ν(OH) is 3540 cm^{-1}, in good agreement with the observed IR band. The remaining bands, generally observed in the Infrared spectrum (3430, 3375, 3335, 3200, 3140 cm^{-1}), could be assigned to the modes originated by the hydrogen bonding (OH…O), which have been found structurally very strong (2.29(2) Å - 2.42(2) Å). For these modes, the DFT calculation gives strong and well structured bands at frequencies (3365, 3350, 3218, 3100 cm^{-1}). At last, it is to note that the distinction between the two types of vibrational modes observed in this spectral region is difficult, and the assignement made here is not considered as rigorously definitive and complete.

3. 3. NMR spectroscopy

The Figure 6 represents the solid-state13C MAS–NMR spectrum of the tetrapropylammonium hydrogen selenate bis (selenic acid). The first peak P1 exhibits a signal located at 8.31 ppm is assigned to the CH_3 groups. Signal P2, which appeared at around 55.47 ppm is due to the CH_2 carbon groups. Finally, signal P3 situated 58.51ppm is attributed to the CH_2 groups. The presence of these peaks suggest the presence of three types of carbon in the structure and also these results are compared to some works which contain these different groups CH_3 and CH_2 [42-43].

3. 4. Hyperpolarizability calculations

The DFT/B3LYP/6-31G(d) was used to calculate the total dipole moment μ, the linear polarizability α and the first hyperpolarizability β. The magnitude of μ_{tot}, α_{tot} and β_{tot} can be calculated using the following equations: [44].

$$\mu_{tot}=\sqrt{\mu_x^2+\mu_y^2+\mu_z^2}$$

$$\alpha_{tot}=\frac{\alpha_{xx}+\alpha_{yy}+\alpha_{zz}}{3}$$

$$\beta_{tot}=\sqrt{(\beta_{xxx}+\beta_{xyy}+\beta_{xzz})^2+(\beta_{yyy}+\beta_{yzz}+\beta_{yxx})^2+(\beta_{zzz}+\beta_{zxx}+\beta_{zyy})^2}$$

The calculated values of the hyperpolarizabilities and the polarizabilities from Gaussian-03 output get been changed from atomic units (a.u.) into electrostatic units (esu). [α: 1 a.u. = 0.1482x10-24esu; β: 1 a.u. = 8.6393x10-33esu]. The electronic dipole moment, the polarizabilities αij and the first hyperpolarizabilities β_{ijk} are listed in Table 10. As shown in this table, the highest value of dipole moment is observed for μ_z component, which is equal to 12.8146D; while for the x and y directions, the obtained values are equal to 0.1703D and -2.2407D, respectively. The calculated total dipole moment is equal to 13.01D. The calculated polarizability α_{tot}, is equal 32.99×10^{-24} esu. The first hyperpolarizability β_{tot} of the material has for value 31.05×10^{-31} eus, which is about 4.5 times more than that of the reference crystal KDP (β_{KDP} = 6.85×10^{-31} eus). The large β value calculated by the DFT/B3LYP/6-31G(d) shows that the synthesized hybrid compound is a good material for NLO applications.

3. 5.Thermal analyses (DTA and TGA)

The thermal behavior of the compound was studied by simultaneous TGA-DTA curves (Figure 7). This type of compound is characterized at the room temperature by its high hygroscopicity [18, 43]. This compound is stable until 368 K; above this temperature, a loss of weight appears. This is owing to the departure of adsorbed water. The endothermic peak observed at T= 440 K is attributed to the melting of the crystal.

3. 6. Electrical properties

To identify the electrical representation of hybrid materials we use some complex electrical parameters such as complex impedance Z* and electrical modulus M*. They are related between them in the following way:

$$Z^* = Z' - jZ'' ;$$

$$M^* = M' + jM''$$

The Figure 8 presents the complex impedance spectra measurements (Z*=Z'- iZ") in the 290-373 K temperature range of $N(C_3H_5)_4[HSeO_4][H_2SeO_4]_2$. When the semicircles move to a lower value of resistance and the centers of these semicircles are on a line below the real axis this is observed when the temperature increases. So the complex impedance spectrum shows that compound follows the Cole-Cole law [45]. The value of α parameter value characterizing the deviation from the Debye law is of the order of 0.103 [46]. We notice that when the temperature increases the resistances gradually decrease. Whereas, the figure 9 be expressed for several temperatures the variation of the imaginary Z" part of the impedance versus frequency Z" = f (log f). The curve displays that the relaxation frequency moves toward high frequency and its intensity reduce when the temperature increases. So this phenomenon shows that the proton became more mobile at high temperature and it proposes that two dispersal mechanisms should be involved [47].

In the range 290-373K, the temperature dependence of the conductivity (ln(σT) versus 1000/T) is given in figure 10. The conductivity of the material was considered from the complex impedance plots at selected temperatures; the plot is explained by Arrhenius type behavior $\sigma T = \sigma_0 \exp(-\Delta E_\sigma/kT)$ where σ_0 is the pre-exponential factor, ΔE_σ is the activation energy for ion migration and k is Boltzmann's constant and T is the absolute temperature. The value of the activation energy ΔE_σ is about 0.40 eV according to the Arrhenius law.

The variation of the bulk relaxation frequency with log(fp) according to the opposite of the temperature (1000/T) shows in figure 11. An Arrhenius-type law ($\sigma T=\sigma_0 \exp(-E_a/K_bT)$ is shown where both lines of conductivity $\log(\sigma_T)$ and modulus peak maxima log(fp) observed in the studied temperature are quasi parallel. Then the activation energies issued from $\log(\sigma_T)$ and $\log(f_p)$ spectra are very close, ($\Delta E_\sigma(LT) = 0.40$ eV; $\Delta_{Ef}(LT) = 0.38$ eV). While the comparison the activation energies values of the compound studied by other similar compounds it is clear to propose that the conductivity is affirmed by the H^+ ion and its transport in the material is possibly owing to a hopping mechanism [48]. The formalism of the complex modulus $M^*= 1/\varepsilon^*= j\omega C_0 Z^*$ was followed in order to optimize the concentration of charge carriers and their frequency hopping and to determine the relaxation times of the conductivity. The curves representing the variation of the imaginary part of the modulus M* normalized by log (f) for different temperatures are reported in figure 12. They appear as asymmetric relaxation peak which the maxima moving towards high frequencies by increasing the temperature. This reflects the increase of disorder from the low temperature phase to the high temperature phase. The area on the left represents the movement to the long distance of the charge carriers, mainly H^+. Close to the relaxation frequency is the area of transition from a long distance movement to a short movement. The real and imaginary parts (M' and M") are deducted by the relation: $M'= \omega C_0 Z"$ and $M"=\omega C_0 Z'$ with $C_0=\varepsilon_0 S/e$; ε_0: permittivity of vacuum ($10^{-11} Fm^{-1}$), S the area and e the thickness of the pellet. The real part of Modulus M' versus log (f) for some temperatures is represented in figure 13 which recognizes the curve $M '= 1/\varepsilon_0$ as asymptote at high frequencies. We can conclude from figure 12 and figure 13 that this behavior confirms the absence of an appreciable electrode polarization in the temperature ranges [47].

4. Concluding remarks

In this study, the synthesis, molecular structure, vibrational study (IR and Raman), optical properties, thermal investigation, NMR of ^{13}C, and electrical properties of the new $N(C_3H_7)_4[HSeO_4][H_2SeO_4]_2$ were described.

The TPSe crystals were successfully obtained by the slow addition of selenic acid H_2SeO_4 to a solution of tetrapropylammonium hydroxide $(C_3H_7)_4NOH$ at room temperature by the slow evaporation.

The title material crystallizes in the monoclinic system with the noncentrosymmetric space group Ia of the. The inorganic $[HSeO_4]^-$ and H_2SeO_4 species consist of infinite two-dimensional inter-linkers via strong hydrogen bonds (O-H…O)

The structural data and the vibrational spectra were calculated by DFT/B3LYP-31G(d) level of theory to support the experimental results discussion. The infrared and Raman studies show the presence of organic and inorganic groups, with good consistency found between the experimental and theoretical IR and Raman spectra.

The polarizability α, the hyperpolarizability β, and the electric dipole μ values were calculated using DFT/B3LYP-31G(d), showing that the TPSe materiel is a good NLO material, and can be improve located for optical applications.

The NMR of ^{13}C spectra declares the solid-state structure resolved by X-ray diffraction.

The electrical measurements of the reported material were studied versus temperature (290 to 363K) and frequency (1 kHz to 100 kHz). The Cole-Cole plots of impedance complex measurements have been performed and analyzed. The ionic transport in the title material is owing to the two movements types: translational hopping of charge carrier and rotational hopping of the $(H_2SeO_4)_2$ and $HSeO_4^-$ anion, and the H^+ via the O-H…O hydrogen bonds.

The result of the thermal study studied by TDA and TGA techniques did not present any phase transition.

Compliance with ethical standards

Conflict of interest On behalf of all the authors, the corresponding author states that there is no conflict of interest.

References

[1] M. Zdanowska-Fraczek, K. Holderna-Natkaniec, Z.J. Fraczek, R. Jakubas, Solid State. Ion. 180 (2009) 9.

[2] I. Chaabane, F. Hlel, K. Guidara, J. Alloys Compd. 461 (2008) 495.

[3] K. Sakai, M. Takemura, Y. Kawabe, J. Lumin. 130 (2010) 2505.

[4] K. Pradeesha, G. Sharachandar Yadava, M. Singhb, G. Vijaya Prakash, Mater. Chem. Phys. 124 (2010) 44.

[5] A. Vishwakarma, P. Ghalsasi, A. Navamoney, Y. Lan, A. Powell, Polyhedron. 30 (2011) 1565.

[6] C. Aruta, F. Licci, A. Zappettini, F. Bolzoni, F. Rastelli, P. Ferro, T. Bezagni, Appl. Phys. A. 81 (2005) 963.

[7] M. Bujak, J. Zaleski, Cryst. Eng. 4 (2001) 241.

[8] K. Karoui, A.B. Rhaiem, K. Guidara, Phys. B. 407 (2012) 489.

[9] K. Bouchouit, E.E. Bendeif, H. EL Ouazzani, S. Dahaoui, C. Lecomte, N. Benali-cherif, B. Sahraoui, J. Chem. Phys. 375 (2010) 1.

[10] H.O. Marcy, M.J. Rosker, L.F. Warren, P.H. Cunningham, C.A. Thomas, L.A. DeLoach, S.P.Velsko, C.A. Ebbers, J.H. Liao, M.G. Kanatzidis, Opt. Lett. 20 (1995) 252.

[11] D.S. Chemla, J. Zyss, Nonlinear Optical Properties of Organic Molecules and Crystals, Academic Press, New York, 1987.

[12] H.O. Marcy, L.F. Warren, M.S. Webb, C.A. Ebbers, S.P. Velsko, G.C. Kennedy, G.C.Catella, Appl. Opt. 31 (1992) 5051.

[13] C.J. Yang, S.A. Jenekhe, Chem. Mater. 6 (1994) 196.

[14] H.S. Nalwa, M. Hanack, G. Pawlowski, M.K. Engel, Chem. Phys. 245 (1999) 17.

[15] J. Baran, M. S´ ledz´, M. Drozd, A. Pietraszko, A. Haznar, H. Ratajczak, J Mol Struct. 526 (2000) 361.

[16] N. L. Speziali, G. Chapuis, Acta Cryst B. 47 (1991) 757.

[17] I. Dhouib, P. Guionneau, Z. Elaoud, J Coord Chemistry. 70 (2017) 3585.

[18] I. Dhouib, H. Feki, P. Guionneau, T. Mhiri , Z. Elaoud, Spectrochim Acta A. 131 (2014) 274.

[19] I. Dhouib, S. Al-Juaid, T. Mhiri, Z. Elaoud, Crystal Structure Theory and Applications. 2 (2013) 8.

[20] D. Abid, I. Dhouib, P. Guionneau, S. Pechev, I. Chaabane, N. Daro, Z. Elaoud, J. Alloys Compd. 824 (2020) 153826.

[21] G. M. Sheldrick SHELXS-97 Programs used for solve crystal structure. University of Gottingen, Germany 1997.

[22] G. M. Sheldrick SHELXL-97 Programs used for crystal structure refinement. University of Gottingen, Germany 1997.

[23] L. J. Farrugia, J Appl 30 (1997) 565.

[24] K. Brandenburg, Diamond Version 2.0 Crystal Impact GbR, Bonn, Germany, 1998.

[25] Gaussian 03, Revision C.02, M.J. Frish, G.W. Trucks, H.B. Schlegel, G.E. Scuseria, M.A. Robb, J.R.Cheeseman, V.G. Zakrzewski, J.A. Montgomery, J.R.E. Stramann, J.C.Burant, S. Dapprich, J.M. Millam, A.D. Daniels, K.N. Kudin, M.C. Stain, O. Farkas, J. Tomasi, V. Barone, M. Cossi, R. Cammi, B. Mennucci, C.Pomelli, C. Adamo, S. Clifford, J. Ochterski, G.A. Petersson, P.Y. Agula, Q. Cui, K. Morkuma, D.K. Malick, A.D. Rabuck, K. Raghavachri, J.B.Foresman, J. Cioslowski, J.V. Ortiz, A.G. Baboul, B.B. Stefanov, G. Liv, A. Liashenko, P. Piskorz, I.Komaromi, R. Comperts, R.L. Martin, D.J. Fox, T. Keith, M.A. Al-Laham, C.Y. Peng, A. Nanayakkaray, M. Challacombe, P.M.W. Gill, B. Johnson,W. Chen,

M.W.Wang, J.L. Andres, C. Gonzalez, M. Head-Gordon, E.S. Replogle, J.A. Pople, Gaussian 03, Revision D.01, Gaussian, Wallingford, 2004.

[26] P. Flukiger, H.P. Luhti, S. Portmann, J. Weber, Molekel 4.2, Swiss Center for Scientific Computing, Manno, Switwerland, 2000–2002.

[27] M. A. Zakharov, S. I. Troyanov, V. B. Rybakov, L. A. Aslanov, E. Kemnitz, Crystallography Reports. 46 (2001) 974.

[28] W. Maalej, Z. Elaoud , T. Mhiri, A. Daoud, A. Driss, Acta Crystallogr Sect E 64 (2008) 2172.

[29] M. Drozd, J. Baran, A. Pietraszko, Spectrochimica Acta Part A. 61 (2005) 2775.

[30] S. I. Troyanov , I. V. Morozov, M. A. Zakharov, E. Kemnitz, Cryst Reports. 44 (1999) 560.

[31] S. Hajlaoui, I. Chaabane, A. Oueslati, K. Guidara, A. Bulou, Spectrochim Acta A. 117 (2014) 225.

[32] N. Hannachi, K. Guidara, A. Bulou, M. Gargouri, F. Hlel, Spectrochimica Acta Part A. 77 (2010) 457.

[33] J. Baran, M. Drozed, T. Lis, M. Sledz, A. J. Barenes, H. Ratajczak; J. of Molecular structure. 372 (1995) 29.

[34] J. Tarasiewicz, R. Jakubas, J. Baran, A. Pietraszko, J Mol Struct. 792 (2006) 265.

[35] F. Hlel, A. Rheim,T. Guerfel, K. Guidara, Zeitschrift fur Naturforschung Section B. 61 (2006) 1002.

[36] A. Ouasri, A. Rhandour, M. C. Dhamelincourt, P. Dhamelincourt, A. Mazzah, Spectrochimica Acta Part A. 58 (2002) 2779.

[37] A. Ben Rhaiem, F. Hlel, K. Guidara, M. Gargouri, Spectrochimica Acta Part A. 66 (2007) 1107.

[38] J. Tarasiewicz, R. Jakubas, J. Baran, A. Pietraszko, J Mol Struct. 697 (2004) 161.

[39] A. Oueslati, F. Hlel, M. Gargouri, Ionics.17 (2011) 91.

[40] M. Gośniowska, Z. Ciunik, G. Bator, R. Jakubas, J. Baran, J Mol Struct. 555 (2000) 243.

[41] A. Oueslati, I. Chaabane, K. Adil, F. Hlel, J of Chemistry. 43 (2013) 5462.

[42] C. Gervais , M. Profeta, V. Lafond, C. Bonhomme, T. Azaïs, H. Mutin, CJ. Pickard, F. Mauri, F. Babonneau, Magn Reson Chem. 42 (2004) 445.

[43] I. Dhouib, A. Ouasri, Z. Elaoud; Journal of Chemical Saudi Society (online 18-06-2020).

[44] G. Keresztury, S. Holly, J. Varga, G. Besenyei, A.Y. Wang, J. R. Durig, Spectrochim Acta A. 49 (1993) 2007.

[45] K. S. Cole, R. H. Cole, J. Chem. Phys. 9 (1941) 341.

[46] J. F. Bauerle, J. Chem. Phys. 30 (1969) 2657.

[47] H. Khemakhem, T. Mhiri, A. Daoud, Solid State Ionics, 117 (1999) 337.

[48] I. Dhouib, P. Guionneau, Z. Elaoud, J. Coord. Chemistry, 70 (2017) 3585.

Figures

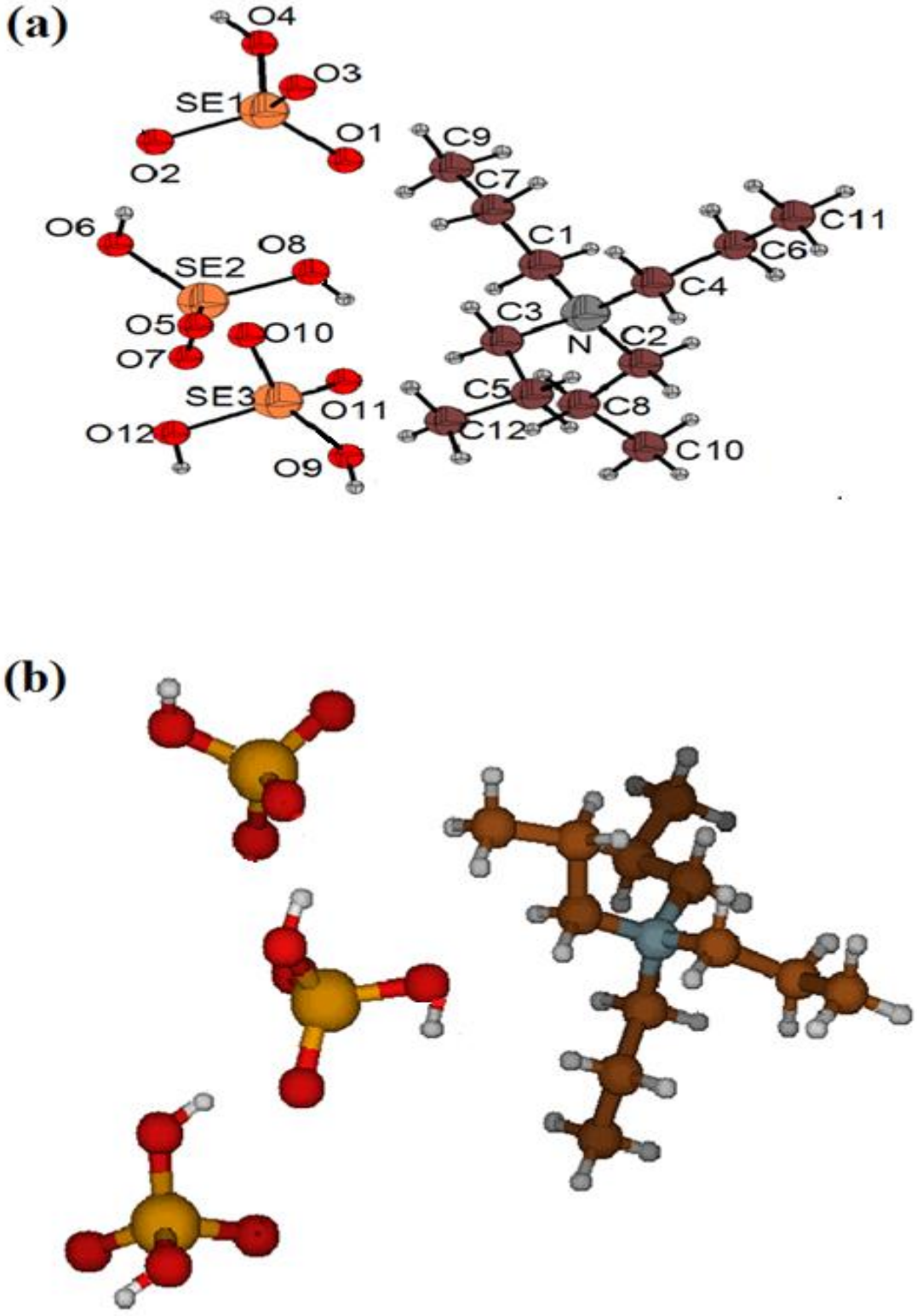

Figure 1: (a) Asymmetric unit (b) B3LYP /6-31G(d) optimized geometry of $N(C_3H_7)_4[HSeO_4][H_2SeO_4]_2$.

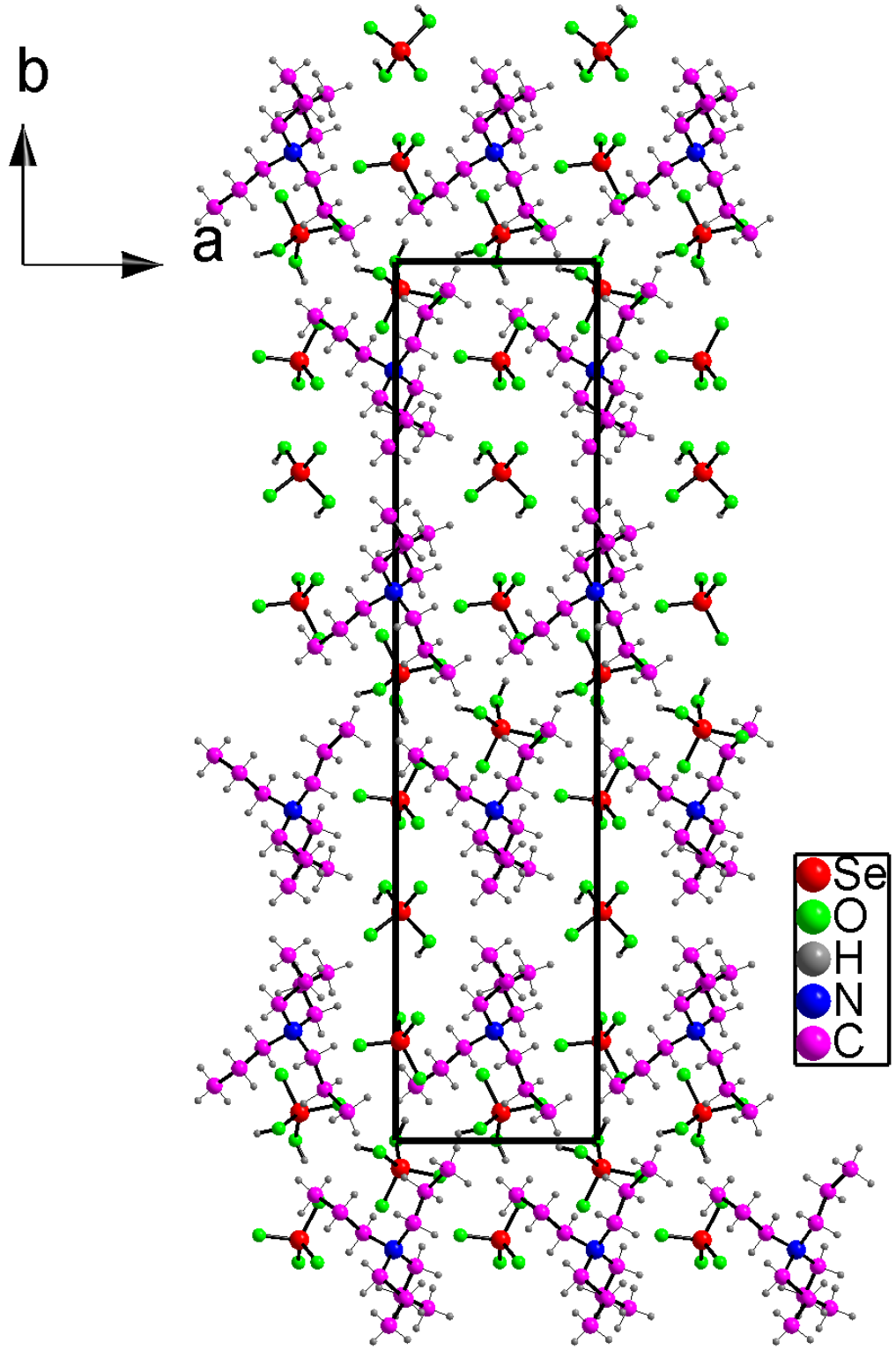

Figure 2: Projection along the b axis of the atomic arrangement of the $N(C_3H_7)_4[HSeO_4][H_2SeO_4]_2$ compound.

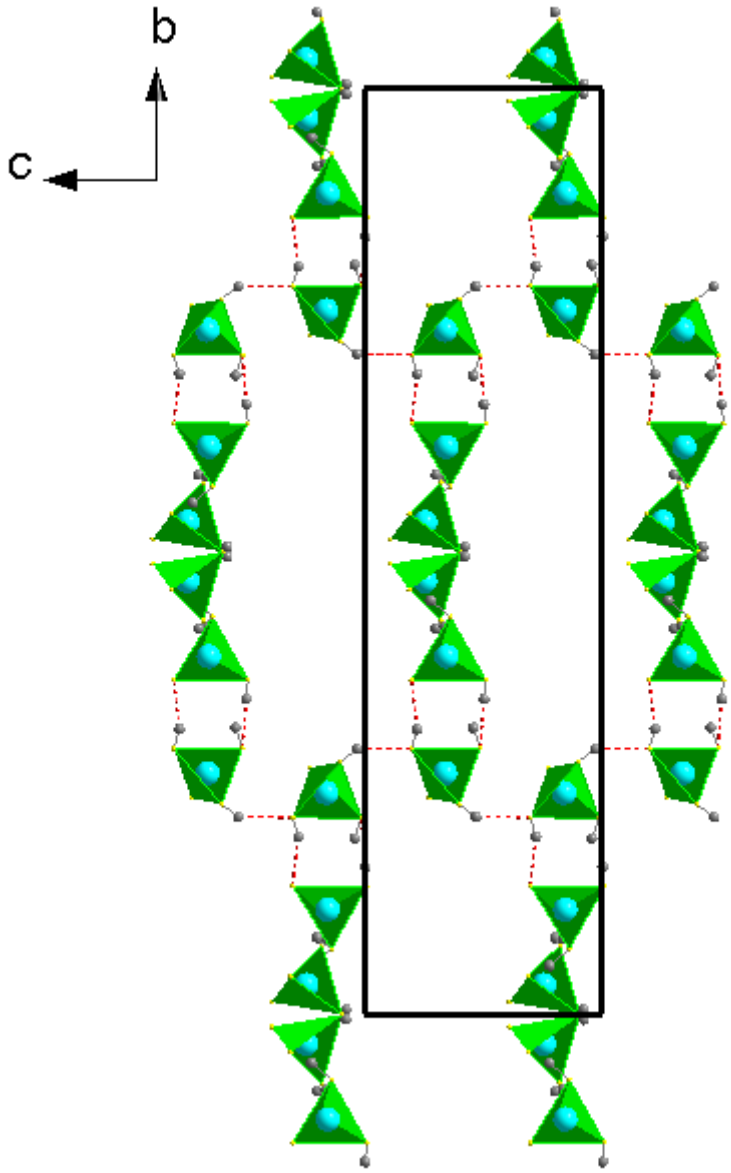

Figure 3: Projection of $[HSeO_4][H_2SeO_4]_2$ structure along the crystallographic B axis.

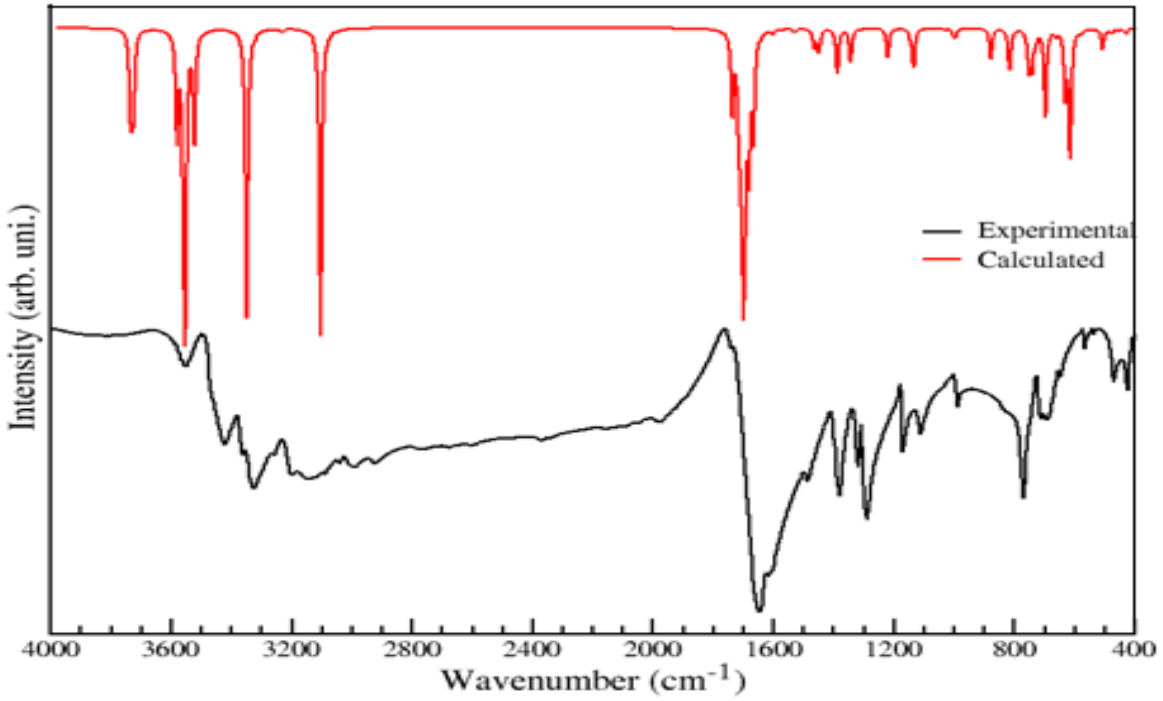

Figure 4: Superposition of (black) the experimental and (red) the DFT computed IR spectra of $N(C_3H_7)_4[HSeO_4][H_2SeO_4]_2$ in the region 400–4000 cm^{-1}.

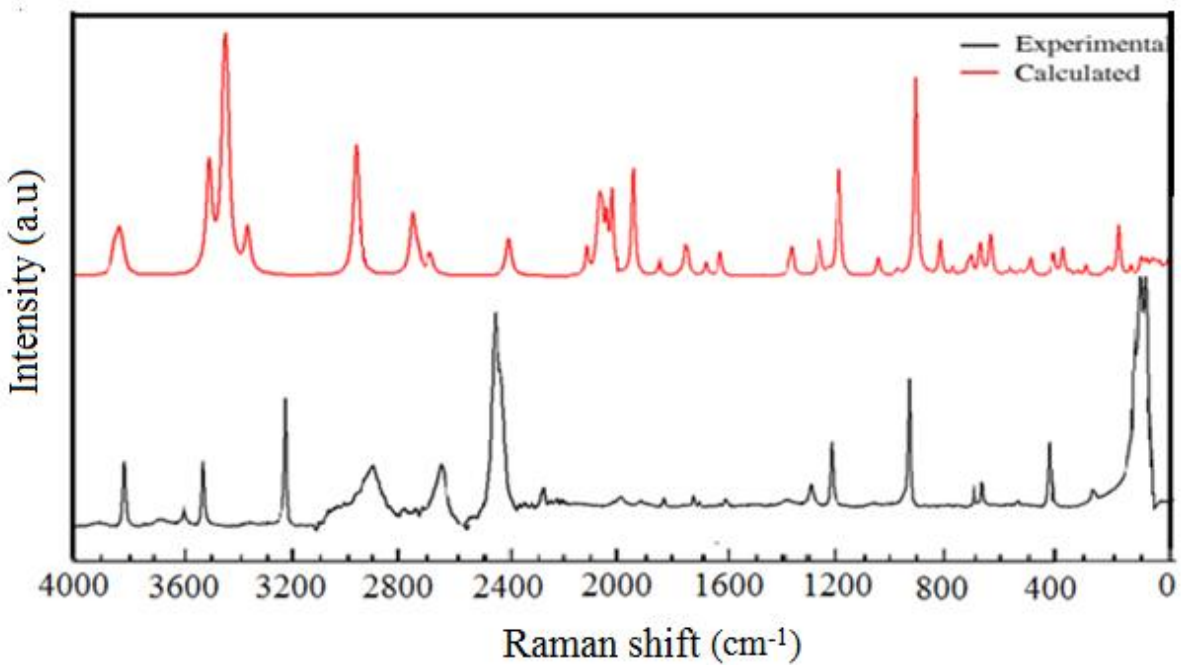

Figure 5: Superposition of (black) the experimental and (red) the DFT computed Raman spectra of $N(C_3H_7)_4[HSeO_4][H_2SeO_4]_2$ in the region 50–4000 cm^{-1}.

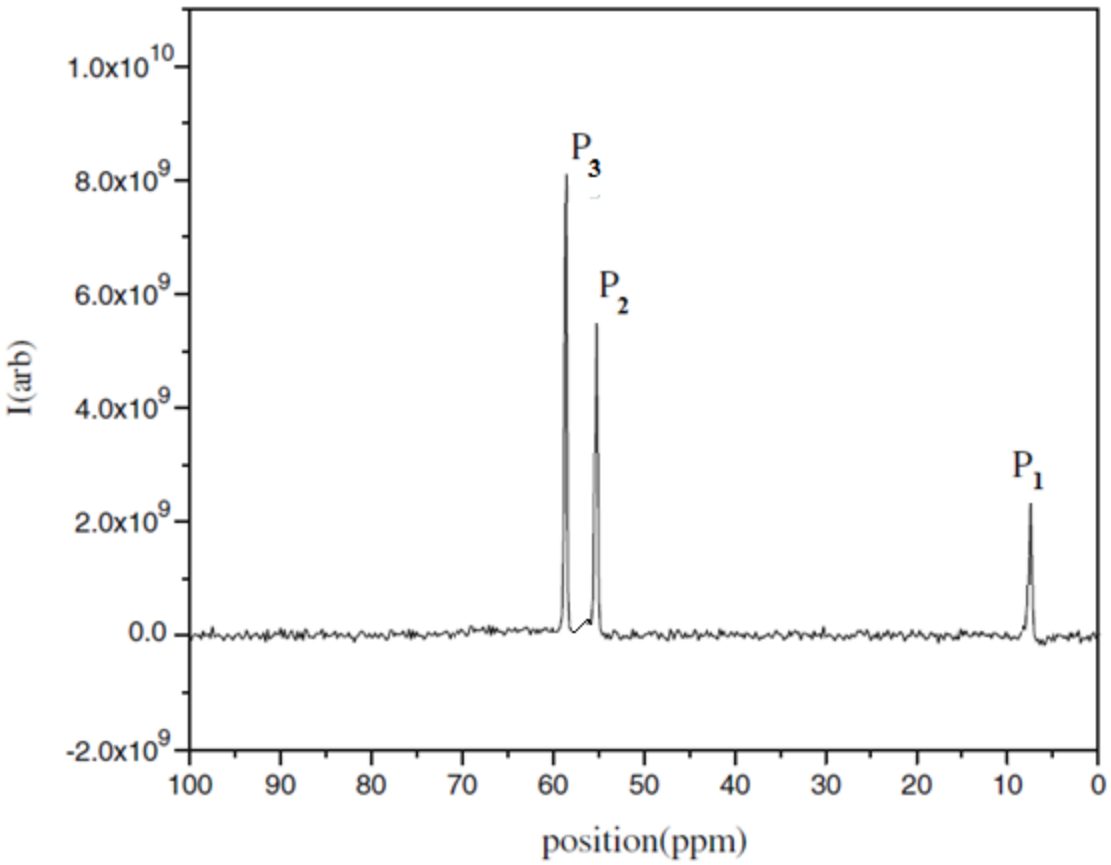

Figure 6: ^{13}C CP–MAS–NMR spectrum of $N(C_3H_7)_4[HSeO_4][H_2SeO_4]_2$.

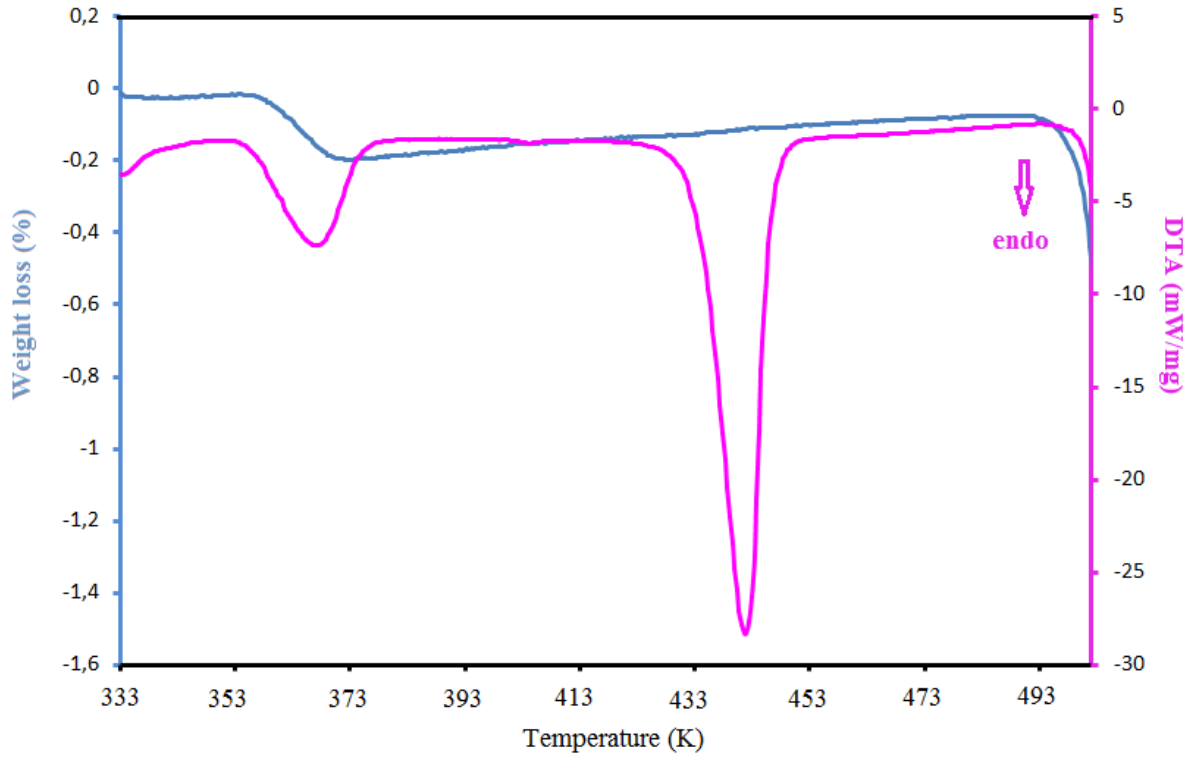

Figure7: Superposition of TGA (pink) and DTA (blue) thermograms of $N(C_3H_7)_4[HSeO_4][H_2SeO_4]_2$

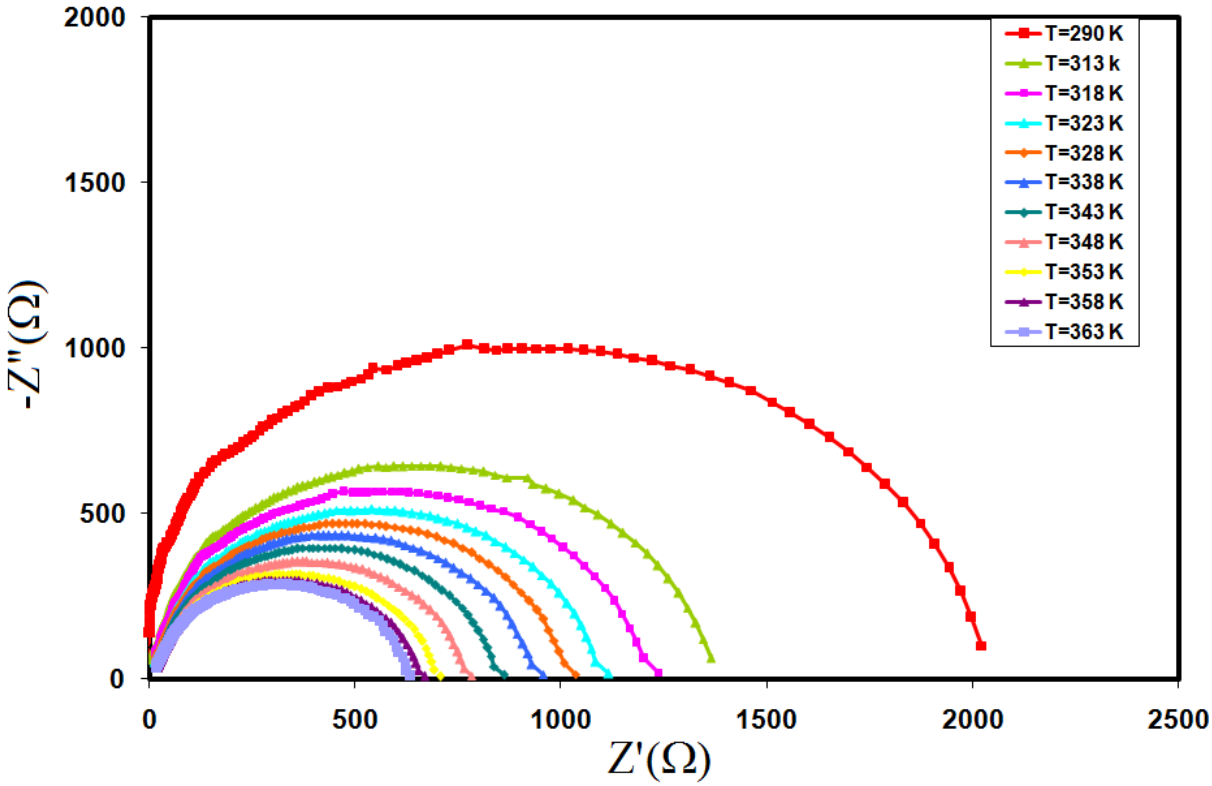

Figure 8: Complex impedance diagrams -Z''(Ω) versus Z'(Ω) of $N(C_3H_7)_4[HSeO_4][H_2SeO_4]_2$ Over the temperature range 290-363 K.

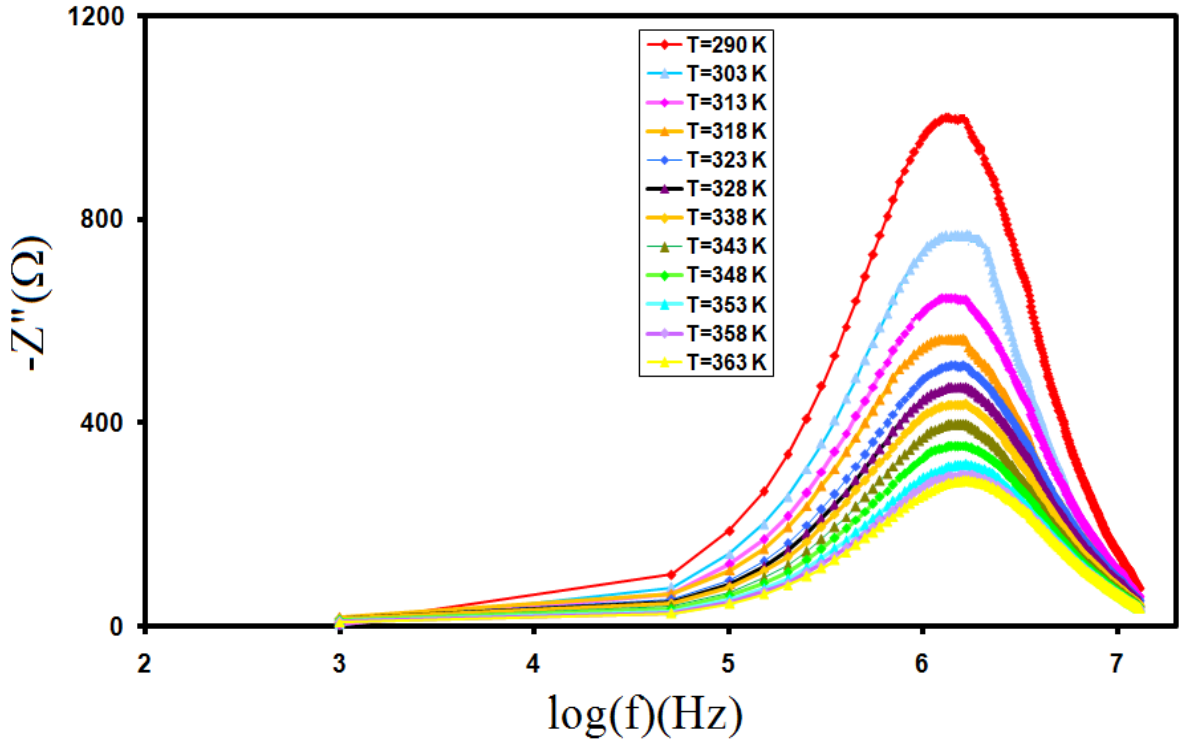

Figure 9: Frequency evolution of the imaginary part of Z for $N(C_3H_7)_4[HSeO_4][H_2SeO_4]_2$ Over the temperature range 290-363 K.

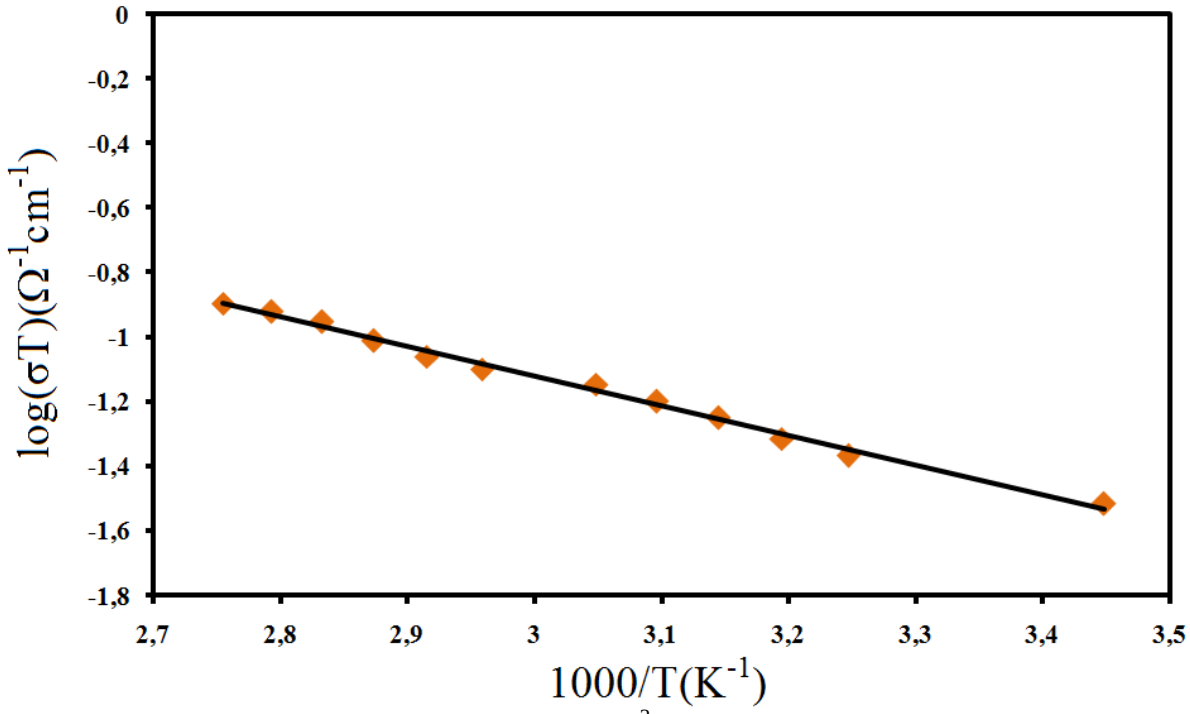

Figure 10: Conductivity plots $\log_{10}(\sigma T) = f(10^3/T)$ of the $N(C_3H_7)_4[HSeO_4][H_2SeO_4]_2$ compound.

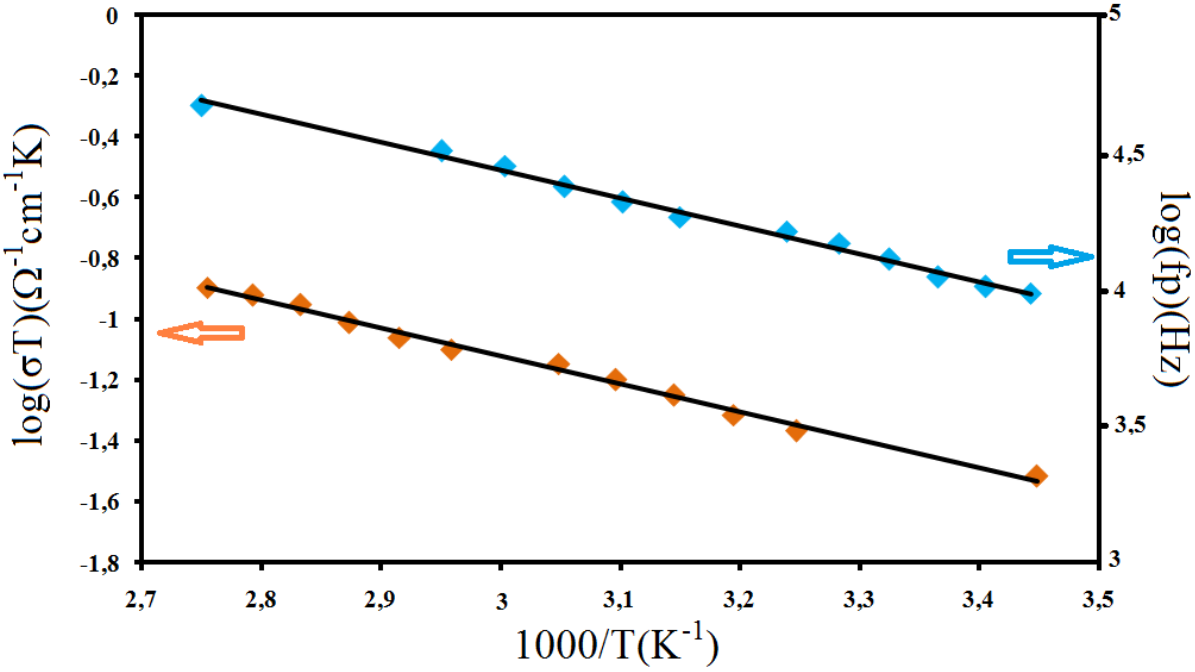

Figure 11: Temperature dependence of log(σT) and log(fp) of the $N(C_3H_7)_4[HSeO_4][H_2SeO_4]_2$ compound

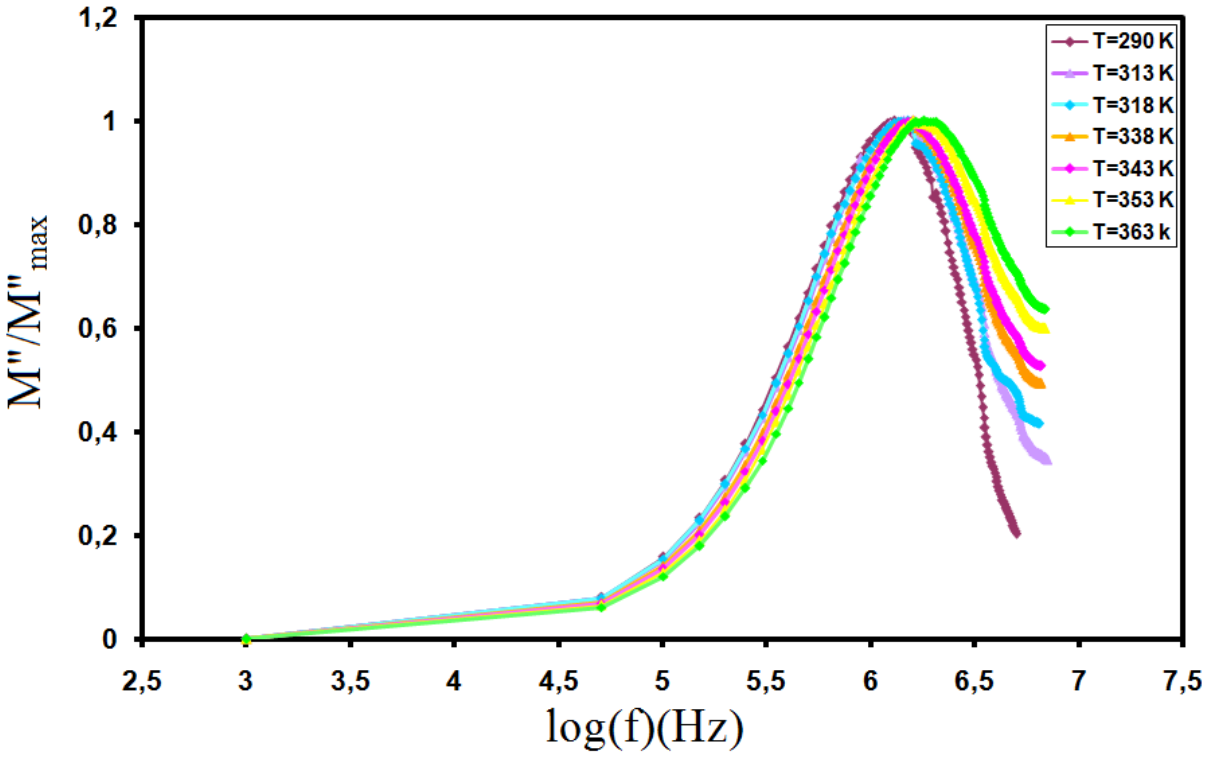

Figure 12: A plot of normalized modulus (M''/M''max) versus log(f) for $N(C_3H_7)_4[HSeO_4][H_2SeO_4]_2$Over the temperature range 290 -363 K.

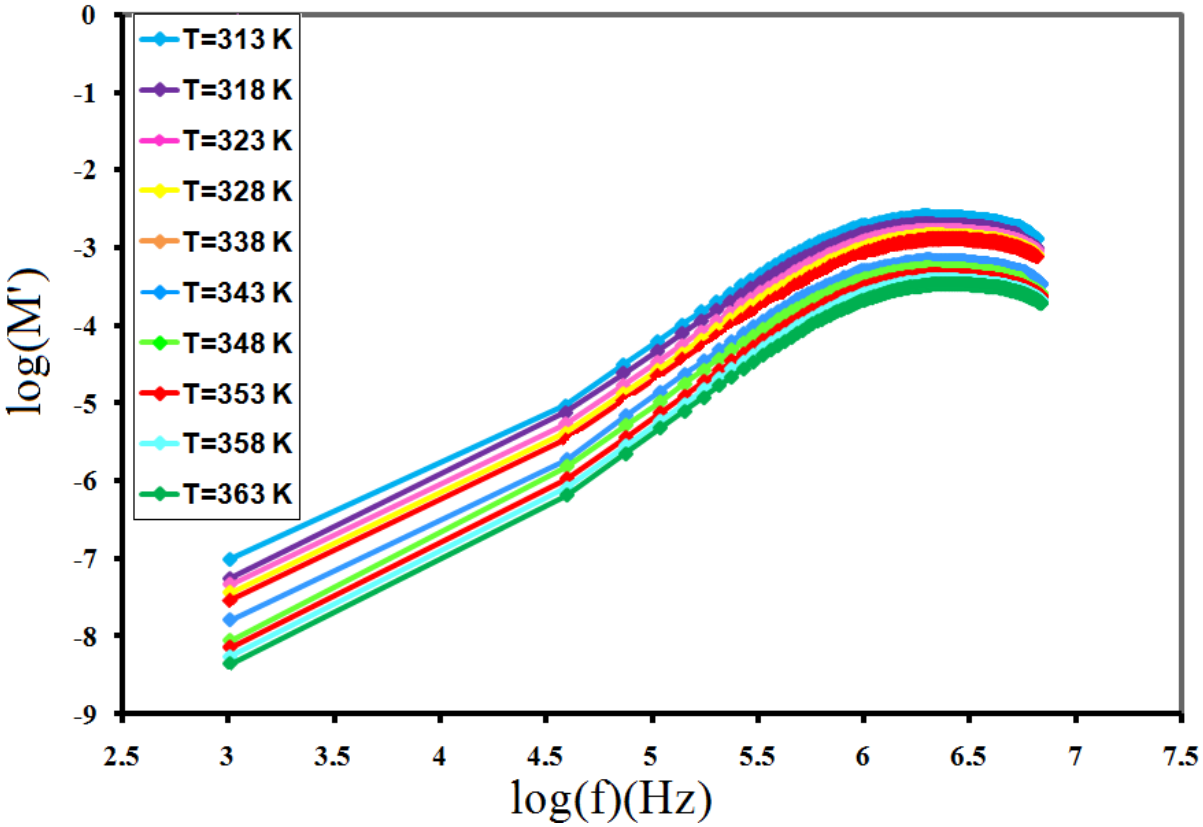

Figure 13: A plot of logM' versus log(f) at various temperature of the $N(C_3H_7)_4[HSeO_4][H_2SeO_4]_2$ compound.

Table 1: Crystal data and structure refinement of the $N(C_3H_7)_4[HSeO_4][H_2SeO_4]_2$ compound.

Formula	**$(C_3H_7)_4N[HSeO_4][H_2SeO_4]_2$**
Color/Shape	Colorless/ Parallelepipedic
Mr (g mol^{-1})	623.3
Crystal system	Monoclinic
Space group	Ia
Density	1.643
Crystal size (mm)	0.28 x 0.17 x 0.10
Unit-cell volume ($A°^3$)	2010.37(8)
Temperature (K)	293(2)
Diffractometer	Kappa CCD
a, *b*, *c* (Å)	7.316(2), 31.763(4), 8.689(2)
α, β, γ (°)	90, 95.34(2), 90
Z	4
Radiation type	Mo K_α
θ range for data collection (°)	$2.1 \leq \theta \leq 27.1$
Reflections measured	2832
Range of *h,k,l*	-3/10, -7/42, -11/11
Reflections with $F_0 > 4\sigma(F_0)$ [b]	1786
GOF	0.952
$R = \sum \|\|F_o\| - \|F_c\|\| / \sum \|F_0\|$	0.0676
Rw	0.1660
Tmin	0.3055
Tmax	0.6067
Computer programs	SHELXS – 97(Sheldrick , 1990)
	SHELXL – 97(Sheldrick , 1997)

Table 2: Comparison between the optimized geometrical parameters and the corresponding experimental data of organic part $[CH_3CH_2CH_2]_4N$

Parameters	**Observed**	**Calculated B3LYP/6-31G(d)**
Bond length (Å)		
N- C1	1.43(2)	1.46
N-C2	1.44(2)	1.42
N -C4	1.45(2)	1.43
N -C3	1.45(2)	1.46
C1- C7	1.38(3)	1.40
C2 -C8	1.47(2)	1.50
C3-C5	1.43(2)	1.42
C4 -C6	1.45(3)	1.43
C5 -C12	1.39(3)	1.41
C6 -C11	1.41(3)	1.42
C7- C9	1.45(3)	1.47
C8 -C10	1.42(3)	1.44
C1- N- C2	114.4(13)	113.8
C1- N -C3	102.5(13)	103.5
C1 -N -C4	112.8(15)	111.9
C2 –N- C3	111.9(13)	111.7
C2- N -C4	105.0(12)	104.4
C4 -N -C3	110.4(12)	109.0
N -C2 -C8	111.6(14)	112.5
N- C4 -C6	119.2(14)	118.0
C5- C3- N	110.5(15)	111.5
C7 -C1- N	121.4(16)	119.6
C1- C7- C9	114(2)	113.7
C10 -C8- C2	105.8(17)	105.0
C11- C6- C4	114.1(17)	113.2
C12- C5- C3	109.4(15)	109.8

Table 3: Comparison between the optimized geometrical parameters and the corresponding experimental data of inorganic part $(HSeO_4)(H_2SeO_4)_2$

Parameters	**Observed**	**Calculated**
Bond length (Å)		**B3LYP/6-31G(d)**
Se1-O1	1.604(12)	1.601
Se1 -O2	1.615(13)	1.611
Se1 -O3	1.559(12)	1.562
Se1- O4	1.617(13)	1.615
O1- Se1- O2	114.7(5)	113.2
O1- Se1- O3	106.3(7)	107.9
O2- Se1 -O3	112.5(7)	111.7
O1- Se1-O4	111.6(7)	110.8
O2 - Se1 -O4	107.1(6)	106.2
O3 - Se1- O4	104.2(7)	105.7
Se2 -O5	1.525(12)	1.526
Se2 -O6	1.649(14)	1.647
Se2- O7	1.556(11)	1.558
Se2- O8	1.598(15)	1.600
O8- Se2- O6	115.5(7)	114.9
O8- Se2 -O7	110.0(8)	109.2
O6- Se2- O7	108.7(7)	107.4
O8 - Se2 -O5	104.4(10)	104.2
O6- Se2- O5	106.1(9)	106.1
O7- Se2- O5	112.1(6)	112.4
Se3- O9	1.650(11)	1.661
Se3- O10	1.602(14)	1.603
Se3- O11	1.523(12)	1.525
Se3- O12	1.647(12)	1.644
O11- Se3- O12	116.2(7)	116.6
O11- Se3- O10	108.8(7)	108.4
O12- Se3 -O10	102.4(8)	101.9
O11- Se3 -O9	105.4(6)	105.1
O12- Se3- O9	112.1(6)	111.1
O10- Se3- O9	112.1(7)	111.8
Se1-Se2	4.006(2)	4.021

Se1-Se3	7.538(4)	7.556
Se2-Se3	4.507(6)	4.521
Se1-N	7.36652)	7.371
Se2-N	6.422(2)	6.427
Se3-N	9.341(3)	9.350

Table 4: Bond lengths (Å) and bond angles (°) in the hydrogen bonding scheme of the $N(C_3H_7)_4[HSeO_4][H_2SeO_4]_2$ compound.

D-H…A	**d(D-H) (Å)**	**d(H…A) (Å)**	**d(D…A) (Å)**	**∠ D-H…A (°)**
O(6)-H(6)...O(2)	0.82	1.62	2,40(2)	158.9
O(8)-H(8)...O(1)	082	1.69	2.35(2)	136.0
O(9)- H(9)...O(7)	0.82	1.52	2.29(2)	156.0
O(12)-H(12)...O(7)^{i}	0.82	1.61	2.42(2)	171.2

Symmetry codes : (i) 1/2+x,-y, z

Table 5: Observed and calculated frequencies (cm^{-1}) of the $N(C_3H_7)_4[HSeO_4][H_2SeO_4]_2$ compound.

Observed		Calculated B3LYP/6-31G*		Assignment
FT-IR	**Raman**	**FT-IR**	**Raman**	
----	3825 m	----	3830	ν (OH)
----	3600 w	----	----	ν (OH)
3540 m	3530 m	3540	3525	ν (OH)
3430 m	----	----	----	ν (OH…O)
3375 sh	----	3365	----	ν (OH…O)
3335 m		3350		ν (OH…O)
3200 w	3230 s	3218	----	ν (OH…O)/ ν (OH)
3140 w, b		3100	----	ν (OH…O)
----	3070 w	----	----	$\nu_{as}(CH_3)$ / $\nu_{as}(CH_2)$
2995 w	----	----		$\nu_{as}(CH_3)$ / $\nu_{as}(CH_2)$
2925 w	2900 m, b	----	2950	$\nu_s(CH_2)$ / $\nu_s(CH_3)$
2365 vw	2650 m 2435 s 2290 w	----	2690 2400	ν (OH----O)
1960 vw	2000 w 1910 vw 1830 vw 1735 w	----- ----- ----- -----	2010 2920 1835 1745	No-fundamental modes
1645 s 1600 s	 1600 vw	1668	----	δ (OH)
1488 m	----	1466	----	$\delta_{as}(CH_3)$ / $\delta_{as}(CH_2)$
1400 m	1393 vw	1407	1385	δ_s (CH_3) / δ_s (CH_2)
1325 m	----	1332	----	t (CH_2)
1300 m	1299 w	----	1280	t (CH_2) / δ (OH)
1195 m	1200 m	1225	1195	ρ_r (CH_3)
1127 w	----	1136	----	ν_{as} (C-N) / ν_{as} (C-C) / ρ_r (CH_3)
1000 w	----	1010	----	γ(OH)
----	920 s	----	910	ν_3 [ν_{as} (Se-O)]
845 vw	----	840	----	ν_1 [ν_s (Se-O)]
765 m	----	760	----	ν (Se–OH) / ν_s (C-N) / ν_s C-C)
700 m, b	705 w	710	700	ν_s (C-N) / ν_s C-C)
650 vw	675 w	630	665	ν_s (C-N) / ν_s C-C)
595 w	----	605	----	δ_{as} (N-C-C) / δ_{as} (C-C-C)
475 w	----	500	----	ν_4 [δ_{as} (O-Se-O)]
425 w	420 m	425	430	ν_4 [δ_{as} (O-Se-O)]
----	275 w	----	----	ν_2 [δ_s (O-Se-O)]
----	100 s	----	----	lattice modes

s: strong, m: medium, w: weak, vw, vey weak, b: broad, sh: shoulder, as: asymmetric; s: symmetric

Table 6: Diagram correlation (C_{2v}--- C_1 --- C_s): Internal vibration modes of H_2SeO_4 group

Molecular Group $\mathbf{C_{2v}}$	Site Group $\mathbf{C_1}$	Factor Group $\mathbf{C_s}$
6 A_1 (Ra, IR) 4 B_1 (Ra, IR) 2 A_2 (Ra) 3 B_2 (Ra, IR)	15 A (IR, Ra)	15 A'(IR, Ra) 15 A''(IR, Ra)

Table 7: Diagram correlation (C_{3v}--- C_1 --- C_s): Internal vibration modes of $[HSeO_4]^-$ group

Molecular Group $\mathbf{C_{3v}}$	Site Group $\mathbf{C_1}$	Factor Group $\mathbf{C_s}$
4 A_1 (Ra, IR) 2 A_2 (Ra) 3 E (Ra, IR)	12 A (IR, Ra)	12A'(IR, Ra) 12 A''(IR, Ra)

Table 8: Illustration of the vibrational modes of $[(H_2SeO_4)_2HSeO_4]^-$ in the crystal.

Species	SeO_4^{2-} modes		OH modes (C_1)
	(T_d)	(C_1)	
2 × (H_2SeO_4)	2 × (A_1 + E + 2F_2)	2 × (9 A)	2 × (6A)
$[HSeO_4]^-$	(3A_1 + 3E)	9 A	3 A
$[(H_2SeO_4)_2HSeO_4]^-$	(5A_1 + 5E + 4F_2)	27 A	15 A

Table 9: Diagram correlation (S_4--- C_1 --- C_s): Internal vibration modes of Tetrapropylammonium group

Molecular Group $\mathbf{S_4}$	Site Group $\mathbf{C_1}$	Factor Group $\mathbf{C_s}$
29 A (Ra) 30 B (Ra, IR) 29 E (Ra, IR)	117 A (Ra, IR)	117 A'(IR, Ra) 117 A''(IR, Ra)

Table 10: The electric dipole moment μ_{tot} (D), the polarizability α ($\times 10^{-24}$ ues) and the first hyperpolarizability β ($\times 10^{-31}$ ues) of $N(C_3H_7)_4[HSeO_4][H_2SeO_4]_2$ computed using DFT//B3LYP/6-31G(d).

μx	0.1703	βxxx	-24.93
μy	-2.2407	βyyy	8.71
μz	12.8146	βzzz	7.63
μ	**13.0101**	βxyy	14.83
αxx	25.58	βxxy	-10.88
αyy	34.6	βxxz	19.73
αzz	38.81	βxzz	0.25
αxy	2.9	βyzz	2.05
αxz	0.68	βyyz	2.09
αyz	0.45	βxyz	2.43
αtot	**32.99**	**βtot**	**31.05**

Figures captions

Figure 1: (a) Asymmetric unit (b) B3LYP /6-31G(d) optimized geometry of $N(C_3H_7)_4[HSeO_4][H_2SeO_4]_2$.

Figure 2: Projection along the c axis of the atomic arrangement of the $N(C_3H_7)_4[HSeO_4][H_2SeO_4]_2$ compound.

Figure 3: Projection of $[HSeO_4][H_2SeO_4]_2$ structure along the crystallographic a axis.

Figure 4: Superposition of (black) the experimental and (red) the DFT computed IR spectra of $N(C_3H_7)_4[HSeO_4][H_2SeO_4]_2$ in the region 400–4000 cm^{-1}.

Figure 5: Superposition of (black) the experimental and (red) the DFT computed Raman spectra of $N(C_3H_7)_4[HSeO_4][H_2SeO_4]_2$ in the region 50–4000 cm^{-1}.

Figure 6: ^{13}C CP–MAS–NMR spectrum of $N(C_3H_7)_4[HSeO_4][H_2SeO_4]_2$.

Figure7: Superposition of TGA (pink) and DTA (blue) thermograms of $N(C_3H_7)_4[HSeO_4][H_2SeO_4]_2$

Figure 8: Complex impedance diagrams -Z''(Ω) versus Z'(Ω) of $N(C_3H_7)_4[HSeO_4][H_2SeO_4]_2$ Over the temperature range 290-363 K.

Figure 9: Frequency evolution of the imaginary part of Z for $N(C_3H_7)_4[HSeO_4][H_2SeO_4]_2$ Over the temperature range 290-363 K.

Figure 10: Conductivity plots $\log_{10}(\sigma T) = f(10^3/T)$ of the $N(C_3H_7)_4[HSeO_4][H_2SeO_4]_2$ compound.

Figure 11: Temperature dependence of log(σT) and log(fp) of the $N(C_3H_7)_4[HSeO_4][H_2SeO_4]_2$ compound.

Figure 12: A plot of normalized modulus (M"/M"max) versus log(f) for $N(C_3H_7)_4[HSeO_4][H_2SeO_4]_2$Over the temperature range 290 -363 K.

Figure 13: A plot of logM' versus log(f) at various temperature of the $N(C_3H_7)_4[HSeO_4][H_2SeO_4]_2$ compound.

Table captions

Table 1: Crystal data and structure refinement of the $N(C_3H_7)_4[HSeO_4][H_2SeO_4]_2$ compound.

Table 2: Comparison between the optimized geometrical parameters and the corresponding experimental data of organic part $[CH_3CH_2CH_2]_4N$.

Table 3: Comparison between the optimized geometrical parameters and the corresponding experimental data of inorganic part $(HSeO_4)(H_2SeO_4)_2$

Table 4: Bond lengths (Å) and bond angles (°) in the hydrogen bonding scheme of the $N(C_3H_7)_4[HSeO_4][H_2SeO_4]_2$ compound.

Table 5: Observed and calculated wavenumbers (cm^{-1}) of the $N(C_3H_7)_4[HSeO_4][H_2SeO_4]_2$ compound.

Table 6: Diagram correlation (C_{2v}--- C_1 --- C_s): Internal vibration modes of H_2SeO_4 group

Table 7: Diagram correlation (C_{3v}--- C_1 --- C_s): Internal vibration modes of $[HSeO_4]^-$ group

Table 8: Illustration of the vibrational modes of $[(H_2SeO_4)_2HSeO_4]^-$ in the crystal

Table 9: Diagram correlation (S_4---C_1---C_s): Internal vibration modes of Tetrapropylammonium group

Table 10: The electric dipole moment μ_{tot} (D), the polarizability α ($\times 10^{-24}$ ues) and the first hyperpolarizability β ($\times 10^{-31}$ ues) of $N(C_3H_7)_4[HSeO_4][H_2SeO_4]_2$computed using DFT//B3LYP/6-31G(d).